DYNAMIC GRIDS FOR FINITE-DIFFERENCE SCHEMES IN MUSICAL INSTRUMENT SIMULATIONS

Silvin Willemsen
Multisensory Experience Lab
Aalborg University Copenhagen
Copenhagen, Denmark
sil@create.aau.dk

Stefan Bilbao, Michele Ducceschi
Acoustics and Audio Group
University of Edinburgh
Edinburgh, UK

Stefania Serafin
Multisensory Experience Lab
Aalborg University Copenhagen
Copenhagen, Denmark

ABSTRACT

For physical modeling sound synthesis, many techniques are available; time-stepping methods (e.g., finite-difference time-domain (FDTD) methods) have an advantage of flexibility and generality in terms of the type of systems they can model. These methods do, however, lack the capability of easily handling smooth parameter changes while retaining optimal simulation quality and stability, something other techniques are better suited for. In this paper, we propose an efficient method to smoothly insert and remove grid points from a FDTD simulation under sub-audio rate parameter variations. This allows for dynamic parameter changes in physical models of musical instruments. An instrument such as the trombone can now be modelled using FDTD methods, as well as physically impossible instruments where parameters such as e.g. material density or its geometry can be made time-varying. Results show that the method does not produce audible artefacts and stability analysis is ongoing.

1. INTRODUCTION

Most musical instruments can be subdivided into an exciter and a resonator component [1]. Examples of exciter-resonator combinations are the bow and violin and the lips and trumpet. In nearly all instruments, the parameters describing the exciter are continuously varied by the performer to play the instrument. As an example, the bow-velocity, position and pressure for the violin, and lip pressure and frequency for the trumpet. Naturally, the resonator is also altered by fingering the strings of the violin or pressing valves on the trumpet to change their pitches. In the real world, however, physical dimensions of the resonators do not change: the string-length stays the same and the total tube length remains unchanged, only the parts that resonate are shortened or lengthened.

While the physical dimensions of the instrument do not change, there are several examples where the parameters of the resonator are also modified. A prime example of this is the trombone, where the tube length is dynamically changed in order to generate different pitches. The slide whistle is another example in this category. Guitar strings are another category where the tension can be smoothly modulated during performance using the fretting finger, a whammy bar or even the tuning pegs directly (see [2]) to create smooth pitch glides. The same kind of tension modulation is used for the membranes of timpani or “hourglass drums" to change the pitch. It is these direct parameter modifications of the resonators that we are interested in to simulate.

Of course, other than simulating existing instruments, one could use potentially simulate instruments that can be manipulated in physically impossible ways. Examples of this could be to dynamically change material properties such as density or stiffness, or even the geometry and size of the instrument where this is physically impossible.

Finite-difference time-domain (FDTD) methods are flexible and generalisable techniques which have recently seen increased use in physical modelling sound synthesis applications [3] though not so recent anymore... The normal approach, for a given system such as a musical instrument, described by a set of partial differential equations (PDEs), is to first represent the instrument over a spatial grid, and then develop a time-stepping method, yielding a fully discrete approximation to the target PDE system.

In many cases, the system itself is static, so that the defining parameters do not change over time. In others, such as the trombone and others mentioned above, this is not the case, and various technical challenges arise when trying to design a simulation using FDTD methods; all relate to the choice of the spatial grid. For example, the grid density is usually closely tied to the parameters themselves through a stability condition. Also, adding and removing points from the grid is nontrivial and can cause audible artefacts and new stability concerns. The default approach of defining a grid globally, according to a very conservative stability condition, as done in [4], is possible, but introduces numerical dispersion and bandlimiting effects. Full-grid interpolation [3, Ch. 5] could be used to change between grid configurations, but extremely high sample rates are necessary to avoid audible artefacts and low-passing effects, rendering any implementation based on this impossible to work in real time.

In this paper, a new method is proposed, allowing the efficient and smooth insertion and deletion of grid points from 1D finite-difference grids to allow for dynamic parameter changes. We are interested in ‘slowly’ varying parameters (sub-audio rate). In a companion paper we present a physical model of the trombone using the method proposed in this paper [5]. Notice that other techniques do allow for dynamic parameter changes but come with their own drawbacks [3]. Examples of dynamic parameters using modal synthesis [6] are shown in [7, 8] and digital waveguides [9] in [10]. maybe another (better) one here

This paper is structured as follows: Section 2 presents the 1D wave equation used as an illustrative for the proposed method. Section 3 gives an introduction to numerical methods, stability and simulation quality. The proposed method for dynamic grids is then presented in Section 4 and applied to the 1D wave equation. Section 5 shows the results of an analysis performed on the method, which are discussed in Section 6. Finally, a conclusion and future perspectives are given in 7.

2. CONTINUOUS SYSTEMS

The wave equation is a useful starting point for investigations of time-varying behaviour in musical instruments. The 1D wave equation may be written as

$$\frac{\partial^2 q}{\partial t^2} = c^2 \frac{\partial^2 q}{\partial x^2}\,, \tag{1}$$

and is defined over spatial domain $x \in [0, L]$, for length L (in m) and time $t \geq 0$ (in s). c (in m/s) is the wave speed. The dependent variable $q = q(x, t)$ in Eq. (1) may be interpreted as the transverse displacement of an ideal string, or the acoustic pressure in the case of a cylindrical tube. Two possible choices of boundary conditions are

$$q(0, t) = q(L, t) = 0 \quad \text{(Dirichlet)}, \tag{2a}$$

$$\frac{\partial}{\partial x} q(0, t) = \frac{\partial}{\partial x} q(L, t) = 0 \quad \text{(Neumann)}, \tag{2b}$$

and describe 'fixed' or 'free' boundary respectively in the case of an ideal string, and 'open' or 'closed' conditions respectively in the case of a cylindrical acoustic tube.

2.1. Dynamic parameters

In the case of the 1D wave equation, only the wave speed c and length L can be altered (in the case of an acoustic tube, only L is variable, and for a string, c could exhibit variations through changes in tension). If Dirichlet-type boundary conditions – as in Eq. (2a) – are used, and under static conditions the fundamental frequency f_0 of the 1D wave equation can be calculated according to

$$f_0 = \frac{c}{2L}. \tag{3}$$

In the dynamic case, and under slow (sub-audiorate) variations of c or L, Eq. (3) still approximately holds. From Eq. (3), one can easily conclude that in terms of fundamental frequency, halving the length of Eq. (1) is identical to doubling the wave speed and vice versa. Looking at Eq. (1) in isolation, f_0 is the only behaviour that can be changed. One can thus leave L fixed and make c dynamic (or time-varying), i.e., $c = c(t)$, which will prove easier to work with in the following section. OK: here, need to refer back to the two primary cases here: the trombone, and the string under variable tensioning, and justify the use of a time-varying c only in these cases. Otherwise this becomes too abstract. I feel like I need to talk about scaling here and how this confirms this statement ($f_0 = \gamma/2$ with $\gamma = c/L$ and scaled space $x \in [0, 1]$). Well, it looks like in the rest of the paper, you've got everything dimensional. Do you want to go for a fully non-dimensional domain $x \in (0, 1)$, so you have γ in there? Then you could deal with this issue right here. hmm.. isn't there something we can say about the 1D wave and how this applies here? I want to keep this general (unscaled).. also as I am going to change L in the trombone paper.. something like "This can more easily be seen if Eq. (1) is scaled or non-dimensionalised as in [3] where $x \in (0, 1)$ and $\gamma = c/L$. To retain generality, we continue with the unscaled case."

3. NUMERICAL METHODS

This section will provide a brief introduction to physical modelling using FDTD methods, including details on stability and quality of the simulations based on these methods.

3.1. Discretisation

In FDTD methods, the first step is the definition of a grid. The spatial variable can be discretised using $x_l = lh$ with integer $l \in [0, \ldots, N]$. distance between two consecutive grid points h (in m), also referred to as the grid spacing, and total number of points $N+1$ (including the boundaries) where the total number of intervals between the grid points is described as

$$N = \lfloor L/h \rfloor, \tag{4}$$

Easier to write this as $h = L/N$, for integer N, so without a flooring operation. hmm.. this flooring operation is important for the comparison with $\mathcal{N}$ (fractional N) later on. Just clearly shows N "integerness" :)OK, but from the above, we don't have $L = Nh$, so the total domain length is off...well, at least for a standard domain!gotcha, I'll figure this out.. (something with (14) perhaps..) with $\lfloor \cdot \rfloor$ denoting the flooring operation. The temporal variable can be discretised using $t_n = nk$ with positive integer n, time step $k = 1/f_s$ (in s) and sample rate f_s (in Hz). The state variable q can then be approximated using $q(x, t) \approx q_l^n$, where grid function q_l^n is the displacement of q at spatial index l and time index n.

The following operators can then be applied to q_l^n to get the following approximations to the derivatives in Eq. (1)

$$\delta_{tt} q_l^n = \frac{1}{k^2}\left(q_l^{n+1} - 2q_l^n + q_l^{n-1}\right) \approx \frac{\partial^2 q}{\partial t^2}\,, \tag{5a}$$

$$\delta_{xx} q_l^n = \frac{1}{h^2}\left(q_{l+1}^n - 2q_l^n + q_{l-1}^n\right) \approx \frac{\partial^2 q}{\partial x^2}\,. \tag{5b}$$

Substituting these definitions into Eq. (1) yields the following finite-difference scheme (FDS)

$$\delta_{tt} q_l^n = c^2 \delta_{xx} q_l^n. \tag{6}$$

Expanding the operators as in (5) and solving for q_l^{n+1} yields the following update equation

$$q_l^{n+1} = 2q_l^n - q_l^{n-1} + \lambda^2 \left(q_{l+1}^n - 2q_l^n + q_{l-1}^n\right). \tag{7}$$

which can be implemented in software. Here,

$$\lambda = \frac{ck}{h} \tag{8}$$

is referred to as the Courant number and determines the stability, as well as the quality and behaviour of the simulation. This will be described in detail in Sections 3.2 and 3.3.

In the FDS described in Eq. (6), the boundary locations are at $l = 0$ and $l = N$. Substituting these locations into Eq. (7) seemingly shows that grid points outside of the defined domain are needed, namely q_{-1}^n and q_{N+1}^n. These can be referred to as *virtual grid points* and can be accounted for using the boundary conditions in Eq. (2). Discretising these yields

$$q_0^n = q_N^n = 0 \quad \text{(Dirichlet)} \tag{9a}$$

$$\delta_{x\cdot} q_0^n = \delta_{x\cdot} q_N^n = 0 \quad \text{(Neumann)} \tag{9b}$$

where

$$\delta_{x\cdot} q_l^n = \frac{1}{2h}\left(q_{l+1}^n - q_{l-1}^n\right) \approx \frac{\partial q}{\partial x} \tag{10}$$

is a second-order accurate approximation of the first-order spatial derivative. The Dirichlet condition in (9a) says that the dis-

placement of q at the boundary locations are always 0. In practice, this means that these grid points do not need to be updated and the spatial range of calculation for Eq. (7) then becomes $l = [1, \dots, N-1]$. If the Neumann condition is used, the boundary points do need to be updated as these are not necessarily 0; rather, their 'slope' is 0. Eq. (9b) can then be expanded to yield defnitions for these virtual grid points

$$q^n_{-1} = q^n_1 \quad \text{and} \quad q^n_{N+1} = q^n_{N-1}\,. \tag{11}$$

Now that the full system is described, the output sound can be retrieved by 'recording' the state q^n_l in Eq. (7) at $0 < l < N$ (when using fixed boundary conditions) and listening to that at the given sample rate f_s.

3.2. Stability

Discretising continuous equations using numerical methods places limits on the parameters describing it. A wrong choice of parameters could render the system unstable and make it "explode". In the case of the update in Eq. (7) it can be shown – using Von Neumann analysis [11] – that the system is stable if

$$\lambda \leq 1, \tag{12}$$

which is referred to as the Courant-Friedrichs-Lewy (CFL) stability condition. The closer λ is to this condition, the higher the quality of the simulation (see Section 3.3) and if $\lambda = 1$, Eq. (7) provides an exact solution to Eq. (1). If $\lambda > 1$ the system will become unstable . Recalling (8), Eq. (12) can be rewritten in terms of grid spacing h to get

$$h \geq ck. \tag{13}$$

This shows that the CFL condition in (12) puts a lower bound on the grid spacing, determined by the sample rate and wave speed. Usually, the following steps are taken to calculate λ

$$h := ck, \;\; N := \left\lfloor \frac{L}{h} \right\rfloor, \;\; h := \frac{L}{N}, \;\; \lambda := \frac{ck}{h}. \tag{14}$$

In other words, condition (13) is first satisfied with equality and used to calculate integer N according to Eq. (4). Thereafter, h is recalculated based on N and used to calculate λ. The calculation of λ in Eq. (14) can be compactly rewritten as

$$\lambda = \frac{ck}{L} \cdot \left\lfloor \frac{L}{ck} \right\rfloor. \tag{15}$$

The flooring operation causes the CFL condition in (12) to not always be satisfied with equality and results in a reduced simulation quality described in the following section.

3.3. Simulation Quality

Choosing $\lambda < 1$ in Eq. (7) will decrease the simulation quality in two ways. Firstly, it will decrease the maximum frequency that the simulation is able to produce, i.e., it will decrease the bandwidth of the output sound of the system.

By analysing the scheme in Eq. (7), it can be shown that the maximum frequency produced by the system can be calculated using $f_{\text{max}} = f_s \sin^{-1}(\lambda)/\pi$ [3, Chap. 6]. Note that only a small deviation of λ from condition (12) already has a profound effect on the bandwidth of the output. Secondly, choosing $\lambda < 1$ causes numerical dispersion. Harmonic partials get closer together at higher frequencies (i.e. get more inharmonic) as λ decreases, which is generally undesirable.

4. THE DYNAMIC GRID

If we want to dynamically change parameters of our model, in this case the wave speed c, there are several aspects that need to be taken into account in a discrete setting. First of all, a change in c causes a change in λ according to Eq. (15), affecting the simulation quality and bandwidth. Secondly, and more importantly, a change in c could result in a change in N through Eq. (4). As N directly relates to the number of grid points, this raises questions as to *where* and especially *how* one would add and remove points to the grid according to the now-dynamic wave speed.

We propose a method that allows for a non-integer number of intervals to smoothly change between grid configurations, i.e, the number of grid points. This removes the necessity of the flooring operation in Eq. (4) and Eq. (15), and consequently satisfies the CFL condition in (12) with equality at all times. Introducing fractional number of intervals $\mathcal{N}$, where $N = \lfloor \mathcal{N} \rfloor$, Eq. (3) can be rewritten in terms of $\mathcal{N}$ by substituting Eq. (4) into Eq. (3) (using Eq. (13) satisfied with equality) yielding

$$f_0 = \frac{1}{2\mathcal{N}k} \quad \text{with} \quad \mathcal{N} = L/h. \tag{16}$$

shouldn't $\mathcal{N}$, h, c, M, M_w all get the n superscript from here onwards? This shows that if $\lambda = 1$, $\mathcal{N}$ solely determines the fundamental frequency of the simulation.

The rest of this section will list the requirements of a method that dynamically changes FDTD grid configurations. Then, the proposed method will be described in detail and summarised, and finally, some details on its implementation are given.

4.1. Method requirements

Ideally, a method that dynamically changes the grid size of finite-difference schemes should

1. generate an output with a fundamental frequency f_0 which is linearly proportional to the wave speed c ($f_0 \propto c$),
2. allow for a fractional number of intervals $\mathcal{N}$ to smoothly transition between different grid configurations
3. generate an output containing $N-1$ modes which are integer multiples of the fundamental ($f_p = f_0 p$ with integer p),
4. work in real time.

The last requirement is added in order to have a playable simulation.

4.2. Proposed Method

In the following, the location of a grid point (in m from the left boundary) i (such as $i = u_0$) at time index n is denoted by x^n_i.

4.2.1. System Setup

Consider two grid functions, $u^n_{l_u}$ and $w^n_{l_w}$ defined over discrete domains $l_u = [0, \dots, M]$ and $l_w = [0, \dots, M_w]$ respectively with integers $M = \lceil 0.5L/ck \rceil$ with $\lceil \cdot \rceil$ denoting the ceiling operation and $M_w = \lfloor 0.5L/ck \rfloor$, i.e., half the number of points allowed by

the stability condition, plus one for overlap. The grid functions can then be placed in line with each other on the same domain x with u_M^n and w_0^n (defined as the inner boundaries) overlapping, i.e., $x_{u_M}^n = x_{w_0}^n = Mh$, and u_0^n and $w_{M_w}^n$ (defined as the outer boundaries) located at $x_{u_0} = 0$ and $x_{w_{M_w}} = L$. See Figure 1a. The following boundary conditions are then imposed:

$$u_0^n = w_{M_w}^n = 0, \quad \text{(Dirichlet)} \tag{17a}$$
$$\delta_x . u_M^n = \delta_x . w_0^n = 0. \quad \text{(Neumann)}, \tag{17b}$$

i.e., the outer boundaries are fixed and the inner boundaries are free. The systems can then be connected at the inner boundaries using a rigid connection

$$u_M^n = w_0^n, \quad \forall n. \tag{18}$$

To sum up, a grid function with N intervals as per Eq. (4) is divided into two separate subsystems connected at their respective inner boundaries.

With the above boundary conditions imposed, the following state vectors can be defined:

$$\mathbf{u}^n = [u_1^n, \ldots, u_M^n]^T, \text{ and } \mathbf{w}^n = [w_0^n, \ldots, w_{M_w-1}^n]^T, \tag{19}$$

with T denoting the transpose operation, and have M and M_w points respectively. Note that the outer boundaries are excluded as they are 0 at all times. The vector concatenating (19) is then defined as

$$\boldsymbol{\mathcal{u}}^n = \begin{bmatrix} \mathbf{u}^n \\ \mathbf{w}^n \end{bmatrix}. \tag{20}$$

Note that the vectors in (19) and (20) also exist at the next $(n+1)$ and previous $(n-1)$ time indices.

Even though the new system has an extra (overlapping) grid point, the behaviour of the new system should be identical to that of the original system. That this holds will be shown below.

Using $u_{l_u}^n$ and $w_{l_w}^n$ in the context of the 1D wave equation, a system of FDSs can be defined as

$$\begin{cases} \delta_{tt} u_{l_u}^n = c^2 \delta_{xx} u_{l_u}^n + J_u(x_{u_M}^n) F \\ \delta_{tt} w_{l_w}^n = c^2 \delta_{xx} w_{l_w}^n - J_w(x_{w_0}^n) F \end{cases} \tag{21}$$

with spreading operators

$$J_u(x_i) = \begin{cases} \frac{1}{h}, & l_u = l_{u,i} = \lfloor x_i/h \rfloor \\ 0, & \text{otherwise} \end{cases} \quad \text{and}$$
$$J_w(x_i) = \begin{cases} \frac{1}{h}, & l_w = l_{w,i} = \lfloor x_i/h \rfloor - M \\ 0, & \text{otherwise} \end{cases} \tag{22}$$

applying the effect of the connection F (in $\mathrm{m}^2/\mathrm{s}^2$) to grid points u_M^n and w_0^n respectively. Expanding the spatial operators in system (21) at inner boundaries u_M^n and w_0^n, recalling the Neumann condition in (17b) and the definition for the virtual grid points needed for this condition in Eq. (11) yields

$$\begin{cases} \delta_{tt} u_M^n = \frac{c^2}{h^2}(2u_{M-1}^n - 2u_M^n) + \frac{1}{h} F \\ \delta_{tt} w_0^n = \frac{c^2}{h^2}(2w_1^n - 2w_0^n) - \frac{1}{h} F. \end{cases} \tag{23}$$

Because of Eq. (18), it is also true that $\delta_{tt} u_M^n = \delta_{tt} w_0^n$, $\forall n$, and F can be calculated by setting the right side of the equations in (23) equal to each other:

$$\frac{c^2}{h^2}(2u_{M-1}^n - 2u_M^n) + \frac{1}{h} F = \frac{c^2}{h^2}(2w_1^n - 2w_0^n) - \frac{1}{h} F,$$
$$F = h \frac{c^2}{h^2}(w_1^n - u_{M-1}^n).$$

Substituting this into system (23) after expansion of the second-time derivative yields the update of the inner boundaries

$$\begin{cases} u_M^{n+1} = 2u_M^n - u_M^{n-1} + \lambda^2(u_{M-1}^n - 2u_M^n + w_1^n) & \text{(24a)} \\ w_0^{n+1} = 2w_0^n - w_0^{n-1} + \lambda^2(u_{M-1}^n - 2w_0^n + w_1^n) & \text{(24b)} \end{cases}$$

which, (again, recalling Eq. (18)) are indeed equivalent expressions for the connected point and is necessary to satisfy the rigid connection. This system can be shown to exhibit behaviour identical to that of the original system. In (24), w_1^n in Eq. (24a) acts as virtual grid point u_{M+1}^n and u_{M-1}^n in (24b) as virtual grid point w_{-1}^n. This important fact is what the method relies on and will be extensively used in the following.

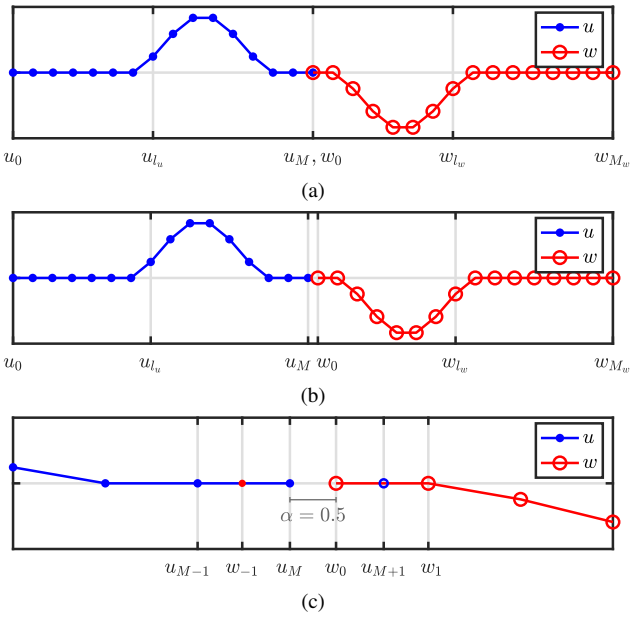

Figure 1: Illustration of the proposed method. In all figures, the x-axis shows the location of the respective grid points, but the x and n are omitted for brevity. (a) Locations of the states of two (1D wave) systems connected at the inner boundaries ($\mathcal{N} = 30$, $x_{u_M}^n = x_{w_0}^n$). (b) When c – and consequently h – are decreased and the positions of the grid points change ($\mathcal{N} = 30.5$, $x_{u_M}^n \neq x_{w_0}^n$). (c) Figure 1b zoomed-in around the inner boundaries. The virtual grid points u_{M+1}^n and w_{-1}^n are shown together with the distance between them expressed using α in Eq. (25).if l_u and l_w are going to be used, don't forget to change in figures (a) and (b)!

4.2.2. *Changing the Grid*

The previous section describes the case in which the stability condition is satisfied with equality, i.e, when L/ck is an integer. The

locations of the outer boundaries $x^n_{u_0}$ and $x^n_{w_{M_w}}$ are fixed, i.e.

$$x^n_{u_0} = x^0_{u_0} = 0 \quad \text{and} \quad x^n_{w_{M_w}} = x^0_{w_{M_w}} = L \quad \forall n.$$

If the wave speed c is then decreased, and consequently the grid spacing h according to Eq. (13) (with equality), all other points move towards their respective outer boundary (see Figure 1b). Calculating h this way allows this method to always satisfy the CFL condition in Eq. (12) with equality.

As mentioned in Section 4.2.1, the state of the virtual grid points at the inner boundaries are defined as $u^n_{M+1} = w^n_1$ and $w^n_{-1} = u^n_{M-1}$ when the inner boundaries are perfectly overlapping (i.e., $x^n_{u_M} = x^n_{w_0}$). If this is not the case (i.e., $x^n_{u_M} \neq x^n_{w_0}$) a Lagrangian interpolator $I(x_i)$ at location x_i from the left boundary (in m) can be used to calculate the value of these virtual grid points (also see Figure 1c for reference). The interpolator I is a row-vector the same length as $\boldsymbol{\mathcal{U}}^n$ (from Eq. (20)) its values depending on what interpolation order is used. In the following the fractional part of $\mathcal{N}$ is defined as

$$\alpha = \alpha^n = \mathcal{N}^n - N^n \tag{25}$$

and for clarity, I and $\boldsymbol{\mathcal{U}}^n$ are indexed by m.

The best behaviour is observed when I is even-ordered (odd-ordered interpolation results in higher-frequency modes increasing as c decreases and vice-versa). Although higher orders yield slightly better behaviour this improvement is negligible and the lowest even-ordered, quadratic interpolation, already yields good results. The quadratic interpolator I_2 is defined as

$$I_2(x_i) = \begin{cases} -(\alpha-1)/(\alpha+1), & m = m_i - 1 \\ 1, & m = m_i \\ (\alpha-1)/(\alpha+1), & m = m_i + 1 \\ 0, & \text{otherwise} \end{cases} \tag{26a}$$

and its flipped version as

$$I_2^{\leftarrow}(x_i) = \begin{cases} (\alpha-1)/(\alpha+1), & m = m_i^{\leftarrow} - 1 \\ 1, & m = m_i^{\leftarrow} \\ -(\alpha-1)/(\alpha+1), & m = m_i^{\leftarrow} + 1 \\ 0, & \text{otherwise} \end{cases} \tag{26b}$$

with $m_i = \lfloor x_i/h \rfloor$ and $m_i^{\leftarrow} = \lfloor x_i/h + (1-\alpha) \rfloor$, where the shift in the latter is necessary to transform the location x_i to the right indices of $\boldsymbol{\mathcal{U}}^n$. When applied to Eq. (20) this yields the definitions for the virtual grid points

$$u^n_{M+1} = I_2^{\leftarrow}(x^n_{u_{M+1}})\boldsymbol{\mathcal{U}}^n = \frac{\alpha-1}{\alpha+1}u^n_M + w^n_0 - \frac{\alpha-1}{\alpha+1}w^n_1 \tag{27a}$$

$$w^n_{-1} = I_2(x^n_{w_{-1}})\boldsymbol{\mathcal{U}}^n = -\frac{\alpha-1}{\alpha+1}u^n_{M-1} + u^n_M + \frac{\alpha-1}{\alpha+1}w^n_0. \tag{27b}$$

As will be shown in Section 5, quadratic interpolation yields the expected fundamental frequency at all times. One can show that when $\mathcal{N}$ is an integer, and thus $\alpha = 0$, Eqs. (27a) and (27b) can be substituted as w^n_1 and u^n_{M-1} into Eqs. (24a) and (24b) respectively (as these acted as virtual grid points u^n_{M+1} and w^n_{-1}). Then recalling Eq. (18) it can be seen that the system reduces to (24) and exhibits the same exact behaviour as the normal case.

Rewriting system (21) to include this yields

$$\begin{cases} \delta_{tt}u^n_{l_u} = c^2\delta_{xx}u^n_{l_u} + J_u(x^n_{u_M})2c^2\delta_{x\cdot}u^n_M \\ \delta_{tt}w^n_{l_w} = c^2\delta_{xx}w^n_{l_w} - J_w(x^n_{w_0})2c^2\delta_{x\cdot}w^n_0 \end{cases} \tag{28}$$

where the definitions for the virtual grid points from the second term are defined by the Neumann boundary condition in Eq. (9b) and those from the last terms are found in Eqs. (27).

4.2.3. Adding and removing Grid Points

When c, and consequently h, is decreased and the inner boundary points surpass the virtual points (i.e. $x^n_{u_M} \leq x^n_{w_{-1}}$ and $x^n_{w_0} \geq x^n_{u_{M+1}}$) and $N^n > N^{n-1}$, a point is added to the right boundary of u and the left boundary of w (for both time indices n and $n-1$) in an alternating fashion:

$$\begin{cases} \mathbf{u}^n = [(\mathbf{u}^n)^T, I_3\mathbf{v}^n]^T & \text{if } N^n \text{ is odd,} \\ \mathbf{w}^n = [I_3^{\leftarrow}\mathbf{v}^n, (\mathbf{w}^n)^T]^T & \text{if } N^n \text{ is even,} \end{cases} \tag{29}$$

where

$$\mathbf{v}^n = [u^n_{M-1}, u^n_M, w^n_0, w^n_1]^T,$$

and cubic Lagrangian interpolator

$$I_3 = \left[-\tfrac{\alpha(\alpha+1)}{(\alpha+2)(\alpha+3)} \quad \tfrac{2\alpha}{\alpha+2} \quad \tfrac{2}{\alpha+2} \quad -\tfrac{2\alpha}{(\alpha+3)(\alpha+2)}\right], \tag{30}$$

with $I_3^{\leftarrow}$ being just a flipped, not shifted, version of (30). See Figure 2. Note, that except in the case of extremely quick parameter

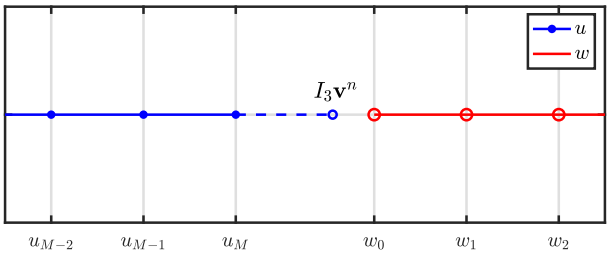

Figure 2: The moment when a point is added to $\mathbf{u}$ at location $x_{u_M} + h$ in Eq. (29). This figure shows an extreme case where this location is far from x_{w_0}, i.e., $\alpha' \not\approx 0$ in Eq. (30).

variations, α in Eq. (30) is expected to be close to zeromeaning that $I_3 \approx [0, 0, 1, 0]$.

Removing grid points happens when c, and consequently h, is increased and $x^n_{u_M} \geq x^n_{w_0}$ (or $N^n < N^{n-1}$). Grid points are simply removed from $\mathbf{u}$ and $\mathbf{w}$ (again for both n and $n-1$) in an alternating fashion according to

$$\begin{cases} \mathbf{u}^n = [u^n_0, u^n_1 ..., u^n_{M-1}]^T & \text{if } N^n \text{ is even,} \\ \mathbf{w}^n = [w^n_1, w^n_2 ..., w^n_{M_w}]^T & \text{if } N^n \text{ is odd.} \end{cases} \tag{31}$$

Until now, only adding and removing points in the center of the system has been considered. This location could be moved anywhere along the grid, the limit being one point from the boundary. In other words, both $u^n_{l_u}$ and $w^n_{l_w}$ need to have at least one point (excluding the outer boundaries). Furthermore, one does not

have to add and remove points from $\mathbf{u}$ and $\mathbf{w}$ in an alternating fashion as in (29), but can just add and remove from (fx.) $\mathbf{u}$ leaving $\mathbf{w}$ the same size throughout the simulation. In the extreme case where $M = N - 1$ and $M_w = 1$ (leaving $w^n_{l_w}$ with only one moving grid point, w^n_0) the method still works.

4.2.4. Displacement correction

A problem that arises from increasing h, is that it is possible that $u^n_M \not\approx w^n_0$ at the time when a grid point needs to be removed. As $x^n_{u_M} \approx x^n_{w_0}$ at the time of removal (except for extremely quick parameter variations), this violates the rigid connection in (18) and causes audible artefacts. A method is proposed that decreases the relative displacement of the inner boundaries the closer their grid-locations are together, i.e., the closer α in (25) is to 0. We thus extend system (28) regular case as

$$\begin{cases} \delta_{tt} u^n_{l_u} = c^2 \delta_{xx} u^n_{l_u} + J_u(x^n_{u_M}) \left(2c^2 \delta_{x\cdot} u^n_M + F_\mathrm{c}\right) \\ \delta_{tt} w^n_{l_w} = c^2 \delta_{xx} w^n_{l_w} - J_w(x^n_{w_0}) \left(2c^2 \delta_{x\cdot} w^n_0 + F_\mathrm{c}\right) \end{cases} \tag{32}$$

Furthermore, using centered temporal averaging and first-order difference operators

$$\mu_{t\cdot} q^n_l = \frac{1}{2}\left(q^{n+1}_l + q^{n-1}_l\right) \tag{33}$$

$$\delta_{t\cdot} q^n_l = \frac{1}{2k}\left(q^{n+1}_l - q^{n-1}_l\right) \tag{34}$$

the correction effect (in $\mathrm{m}^2/\mathrm{s}^2$)

$$F_\mathrm{c} = \beta\left(\omega_0^2 \mu_{t\cdot} \eta^n + \sigma_0 \delta_{t\cdot} \eta^n\right). \tag{35}$$

with the difference in displacement between the inner boundaries

$$\eta^n \triangleq w^n_0 - u^n_M \tag{36}$$

(in m), (angular) frequency of the spring ω_0 (in s^{-1}) and damping coefficient σ_0 (in s^{-1}). Furthermore, $\beta = \beta(\alpha)$ scales the effect of the displacement correction and is defined as

$$\beta = \frac{1-\alpha}{\alpha + \varepsilon}, \tag{37}$$

(in m) for the units to make sense... I guess it includes the $1/\rho A$ (for a 1D wave modelling a string without stiffness) but as it is an artificial connection force, it might make more sense to exclude all units here.. where $\varepsilon \ll 1$ prevents a division by 0. Despite Eq. (33), it is possible to calculate the force explicitly (such as in [3] or [12]). Furthermore, it can be shown that this calculation is defined, even for $\alpha = \varepsilon = 0$ which acts as a rigid connection such as Eq. (18).

4.3. Summary

Here, Section 4.2 is summarised and describes the final version of the proposed method.

The proposed method subdivides a grid function q^n_l with $N+1$ grid points into two grid functions $u^n_{l_u}$ and $w^n_{l_w}$ with $M+1$ and M_w+1 grid points respectively for a total of $N+2$ grid points. Knowing that $\lambda = 1\ \forall n$, Eq. (7), written for both grid functions, becomes

$$u^{n+1}_{l_u} = u^n_{l_u+1} + u^n_{l_u-1} - u^{n-1}_{l_u}, \tag{38a}$$

$$w^{n+1}_{l_w} = w^n_{l_w+1} + w^n_{l_w-1} - w^{n-1}_{l_w}. \tag{38b}$$

Due to the Dirichlet boundary condition in (9a) imposed on the outer boundaries of the system, u^n_0 and $w^n_{M_w}$ are 0 at all times and do not have to be included in the calculation. The ranges of calculation for Eq. (38a) and (38b) then become $l_u = [1, \ldots, M]$ and $l_w = [0, \ldots, M_w - 1]$ respectively.

The inner boundaries are calculated by expanding (28) (ignoring the displacement correction for now)

$$u^{n+1}_M = u^n_{M+1} + u^n_{M-1} - u^{n-1}_M, \tag{39a}$$

$$w^{n+1}_0 = w^n_{-1} + w^n_1 - w^{n-1}_0. \tag{39b}$$

where virtual grid points u^n_{M+1} and w^n_{-1} can be calculated using Eq. (27).

Then, when $N^n > N^{n-1}$ a point is added to $\mathbf{u}^n$ and $\mathbf{u}^{n-1}$ (or $\mathbf{w}^n$ and $\mathbf{w}^{n-1}$) using Eq. (29), and when $N^n < N^{n-1}$ a point is removed from the same vectors using Eq. (31). In order to prevent audible artefacts when increasing c (and thus decreasing $\mathcal{N}$), a method in (32) is proposed to ensure that the inner boundaries have a similar displacement when one of them is removed.

Finally, using $\boldsymbol{\mathcal{U}}$ from Eq. (20) the total system can be compactly written in matrix form as

$$\mathbf{C}_+ \boldsymbol{\mathcal{U}}^{n+1} = \mathbf{B}\boldsymbol{\mathcal{U}}^n + \mathbf{C}_- \boldsymbol{\mathcal{U}}^{n-1} \tag{40}$$

with $N \times N$ matrices

$$\mathbf{B} = \left[\begin{array}{ccc|ccc} \ddots & \ddots & & & & 0 \\ 1 & 0 & 1 & & & \\ & 1 & \frac{\alpha-1}{\alpha+1} & 1 & -\frac{\alpha-1}{\alpha+1} & \\ \hline & -\frac{\alpha-1}{\alpha+1} & 1 & \frac{\alpha-1}{\alpha+1} & 1 & \\ & & & 1 & 0 & 1 \\ 0 & & & & \ddots & \ddots \end{array}\right] \tag{41}$$

containing the effect of the general method described in Section 4.2.2 and

$$\mathbf{C}_\pm = \pm\left(\mathbf{I} - \frac{\beta k^2(\omega_0^2 \pm \sigma_0/k)}{2}\mathbf{J}\boldsymbol{\eta}\right) \tag{42}$$

containing the effect of the displacement correction described in Section 4.2.4 where $\mathbf{I}$ is the $N \times N$ identity matrix and

$$\mathbf{J} = [\mathbf{0}_{M-1}, 1/h, -1/h, \mathbf{0}_{M_w-1}]^T \tag{43}$$

and

$$\boldsymbol{\eta} = [\mathbf{0}_{M-1}, -1, 1, \mathbf{0}_{M_w-1}] \tag{44}$$

are vectors of length N and $\mathbf{0}_i$ is a zero-vector of length i. Notice that as α approaches 1, $\mathbf{B}$ reduces to a matrix with ones on the diagonals next to the main diagonal and zeros elsewhere, which translates directly to the normal case in Eq. (7) with $\mathcal{N} = M + M_w + 1$.

4.4. Implementation

Algorithm 1 shows the order of calculation to implement the method presented in this paper. Important is to only retrieve a change in c

at time index n before all other, so that $u^n_{l_u}$ and $w^n_{l_w}$ are calculated with the same α and β time index n for all l_u and l_w.

while *application is running* **do**
- Retrieve new c
- Calc. h (Eq. (13) with equality)
- Calc. $\mathcal{N}^n$ and N^n (Eqs. (16) and (4))
- Calc. α (Eq. (25))
- **if** $N^n \neq N^{n-1}$ **then**
  - Add or remove point (Eq. (29) or (31))
  - Update M and M_w
- **end**
- Calc. β (Eq. (37))
- Update $\mathbf{B}$ and $\mathbf{C}_\pm$ (Eqs. (41) and (42))
- Calc. scheme (Eq. (40))
- Retrieve output
- Update states ($\boldsymbol{\mathcal{U}}^{n-1} = \boldsymbol{\mathcal{U}}^n, \boldsymbol{\mathcal{U}}^n = \boldsymbol{\mathcal{U}}^{n+1}$)
- Update N ($N^{n-1} = N^n$)
- Increment n

end

Algorithm 1: Pseudocode showing the order of calculations.

5. ANALYSIS AND RESULTS

This section shows the analysis of the system presented in the previous section and its behaviour.

5.1. Energy Added this for your (SB, MD) review

I guess the most important thing I want to highlight using this section is the fact that in the static case, the energy can be shown to be constant, even when $\alpha \neq 0$. This means that the proposed method (without displacement correction) does not introduce losses! My question to you: do you see a way (perhaps from the last terms in system (28) or the boundary terms in Eq. (48)) to prove that the total energy of the system is static when α is static?

The energy of system (28) (which after expansion at the inner boundaries simply becomes (39)) can be retrieved using energetic analysis techniques [3] and a weighted inner product yielding

$$\delta_{t+}\left(\mathfrak{h}_u + \mathfrak{h}_w\right) = \mathfrak{b}_u + \mathfrak{b}_w \tag{45}$$

with

$$\begin{aligned}\mathfrak{h}_u = \frac{1}{2}\sum_{l_u=0}^{M-1} h\Big((\delta_{t-}u^n_{l_u})^2 + c^2(\delta_{x+}u^n_{l_u})(\delta_{x+}u^{n-1}_{l_u})\Big) \\ + \frac{\epsilon}{4}h(\delta_{t-}u^n_M)^2,\end{aligned} \tag{46}$$

$$\begin{aligned}\mathfrak{h}_w = \frac{1}{2}\sum_{l_w=1}^{M_w} h\Big((\delta_{t-}w^n_{l_w})^2 + c^2(\delta_{x-}w^n_{l_w})(\delta_{x-}w^{n-1}_{l_w})\Big) \\ + \frac{\epsilon}{4}h(\delta_{t-}w^n_0)^2,\end{aligned} \tag{47}$$

and

$$\begin{aligned}\mathfrak{b}_u &= c^2(\delta_{t\cdot}u^n_M)\left((\delta_{x-}u^n_M) + \frac{\epsilon}{2}h(\delta_{xx}u^n_M)\right) \quad \text{and} \\ \mathfrak{b}_w &= c^2(\delta_{t\cdot}w^n_0)\left(-(\delta_{x+}w^n_0) + \frac{\epsilon}{2}h(\delta_{xx}w^n_0)\right)\end{aligned} \tag{48}$$

with $\epsilon = \alpha + 1$. When $\alpha = 0$, $u^n_M = w^n_0$ and the boundary terms vanish. When $\alpha \to 1$ the boundary terms reduce to

$$\mathfrak{b}_u + \mathfrak{b}_w = -\frac{c^2}{2}\delta_{t+}\big(h(\delta_{x+}u^n_M)(\delta_{x+}u^{n-1}_M)\big), \tag{49}$$

which is essentially the potential energy between the inner boundaries. See Appendix B.4 (p. 17) in `https://www.overleaf.com/project/5eec78b95071c2000121fff4` for a derivation.

5.2. Modes

A modal analysis can be performed on system (40) while changing c to obtain the frequencies and damping coefficients for each mode. As a test case, the wave speed of a system running at $f_s = 44100$ Hz is dynamically varied from $c = 2940$ ($\mathcal{N} = 15$) to $c = 2205$ ($\mathcal{N} = 20$). The results of the analysis are shown in Figure 3a where higher damping (induced by the displacement correction) is indicated using thinner and bluer lines. Figure 3b shows the resulting spectrogram, with the displacement correction deactivated, of the system excited with $u^0_1 = 1$ and the output retrieved at u^n_1, and Figure 3c shows a system with the same excitation but the change in c inverted ($\mathcal{N} = 20 \to 15$) and displacement correction activated.

In the following, the lowest mode generated by the analysis is referred to as f_1 and should ideally be equal to f_0 calculated using Eq. (3). The first thing one can observe from Figure 3a is that the frequencies of the modes decrease as c decreases (as desired). The lower the mode, the more linear this decrease happens. Between $\mathcal{N} = 15$ and $\mathcal{N} = 16$, f_1 maximally deviates by -0.15 cents. In this same interval f_{15} maximally deviates by -67 cents. This deviation gets less as $\mathcal{N}$ increases. Experiments with higher even-ordered Lagrange interpolators shows that these frequency deviations become smaller, but not by a substantial amount. The quadratic interpolator has thus been chosen for being simpler and more flexible while not being substantially worse than higher order interpolators.

Another observation from Figure 3a is that there are always N modes present, corresponding to the number of moving points of the system. As can be seen from the spectrum in Figure 3b the highest mode is not excited. If the system is excited when $\mathcal{N}$ is not an integer, the highest mode will also be excited. When an implementation of the system using this method with integer $\mathcal{N}$ (static) is compared to a normal implementation of the 1D wave equation (shown in Section 3) with the same value N, identical outputs are observed, even though the latter has $N - 1$ moving points. this confirms that (40) reduces to the normal case when $\alpha = 0$

Using the quadratic interpolation from (27), or any other even-ordered Lagrange interpolator for that matter, the modal frequencies of the system do not change based on location. Experiments done with odd-ordered Lagrange interpolators showed that better behaviour is observed when points are added / removed closer to the boundaries.

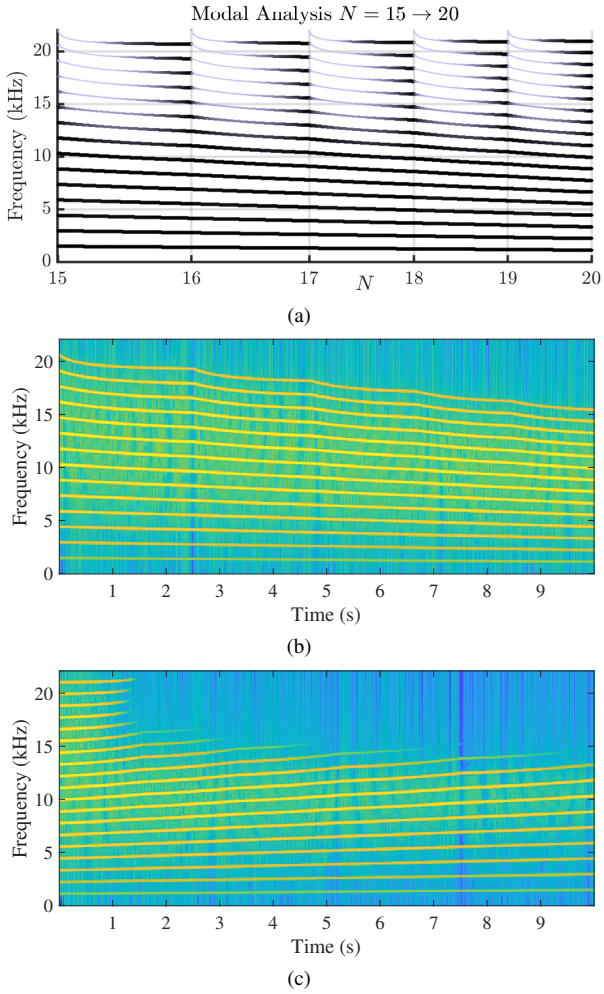

Figure 3: Experiments showing (linearly) varying wave speed between $c = 2940$ ($\mathcal{N} = 15$) and $c = 2205$ ($\mathcal{N} = 20$) with $M = N - 1$ and $M_w = 1$ running at $f_s = 44100$ Hz. (a) Modal analysis of system (40). Thinner and bluer lines indicate a higher amount of damping. (b) Output of the system while decreasing c ($\mathcal{N} = 15 \rightarrow 20$) without displacement correction, excited with a narrow raised cosine at $n = 0$ retrieved at u_1^n. The sound output follows the same pattern as predicted by the analysis shown in Figure 3a. (c) Output of the system while increasing c ($\mathcal{N} = 20 \rightarrow 15$) with displacement correction activated (essentially flipping the analysis in Figure 3a along the x-axis). Higher frequencies are filtered out and prevent artefacts.

5.3. Displacement Correction

In the experiments, parameters in Eq. (35) are set to $\omega_0 = \sigma_0 = 1$. The displacement correction has a low-pass comb filtering effect on the system, where the position and amount of notches directly relates to the position of where grid points are added and removed. The best behaviour, i.e., least affecting lower frequencies, is when $M = N - 1$ and only has one notch as shown in Figures 3a and 3c.

Experiments with different rates of change in c showed that artefacts appeared when the highest mode is not attenuated as a grid point is removed.

5.4. Limit on Rate of Change of c

The current implementation of the proposed method can only add or remove a maximum one point per sample using Eqs. (29) and (31). The speed of decreasing f_0 according to (16) is thus limited by $|\mathcal{N}^n - \mathcal{N}^{n-1}| \leq 1$. Though this is the maximum limitation on speed, a much lower limitation needs to be placed to keep the system well-behaved. The usual stability and energy analyses performed on FDSs are not valid anymore in the time-varying case. Frozen coefficient analysis as in [11] could be applied here and hold for slowly varying coefficients, but is left for future work.

6. DISCUSSION

To decide whether the proposed method works satisfactory, the results presented in the previous section are compared to the method requirements listed in Section 4.1 (denoted by r# for short).

It can be argued that the frequency deviations of f_1 from f_0 are sufficiently small to say that the r1 is satisfied. As for r2, a fractional number of intervals $\mathcal{N}$ has been introduced and smooth transitions are indeed observed from Figure 3b, in the case when c is decreased and $\mathcal{N}$ is increased. When c is increased instead, the displacement correction prevents artefacts when grid points are removed as seen in Figure 3c. However, the filtering effect that the displacement correction has on the system (mentioned in Section 5.3) is not ideal as it creates notches in the spectrum of the output sound. The least intrusive filtering happens when points are added and removed as close to the boundary as possible, i.e., when $M = 1$ or $M_w = 1$ where the notch only occurs in the higher end of the spectrum. As mentioned, artefacts are already removed when the highest mode is attenuated when a grid point is removed, so the current choice for ω_0 and σ_0 in Eq. (35) might be too high. As the displacement correction acts as a filtering operation, higher speeds of parameter variation will possibly cause the highest mode to not be filtered out 'in time'. The values of ω_0 and σ_0 could therefore be made dependent on the rate of change of c to have a higher effect when c is increased faster and vice versa. Either way, as this is still not ideal, another method for reducing artefacts that less affects the frequency content of the system should be devised, if possible.

The modal analysis in Figure 3a shows that method generates N rather than $N - 1$ modes as set by r3. However, the output does contain the correct number of modes as shown in Figure 3b due to the highest mode not being excited. This is a result of the rigid connection imposed on the inner boundaries, forcing them to have the same displacement and act as one point. As mentioned in the results, when the system is excited at a non-integer $\mathcal{N}$, the highest mode is excited due to the fact that the inner boundaries can have different displacements in that case, but this is not an issue. The latter part of r3, however, is not satisfied. The modes deviate from integer multiples of f_0, moreso for higher modes. Other interpolation techniques could be investigated to improve the behaviour and decrease this deviation.

Finally, the method only adds a few extra calculations for the inner boundaries so r4 is also easily satisfied.

Although the results bring forward some drawbacks of the proposed method, such as modal frequency deviations, and filtering effects, most of these happen affect the higher frequencies

of the output. First of all, human frequency sensitivity becomes very limited above 3000 Hz [13] making high-frequency deviations much less important perceptually. Secondly, the physical systems one usually tries to model contain high-frequency losses, causing higher modes to usually not have very high amplitudes to begin with. Finally, $\mathcal{N}$ is usually much bigger in the systems that one tries to model, with which frequency deviations happen to a much smaller degree.

7. CONCLUSIONS AND PERSPECTIVES

This paper presents a method to change grid configurations of finite difference schemes to allow for dynamic parameter changes. Grid points are shown to be added and removed smoothly and do not cause artefacts when switching between between grid configurations.

The proposed method might not provide an exact solution to the problem, but does circumvent the need for upsampling and higher orders of computations necessary to approximate this solution. Furthermore, the method allows the stability condition, which the scheme needs to abide, to always be satisfied with equality. This allows for a simulation where the parameters can be changed dynamically without running into either stability or quality issues, at least at slow parameter changes.

Although this method has only been applied to the the 1D wave equation it could be applied to many other 1D FDSs. Other parameters, such as material density or stiffness could also be made dynamic, going beyond what is physically possible. An application of the method that could be investigated is that of non-linear systems, such as the Kirchhoff-Carrier string model [14] where the tension is modulated based on the state of the system.

Other future work includes creating an adaptive version of the displacement correction that changes its effect depending on the speed at which the grid is changed. Finally, stability and energy analyses will have to be performed to test the limits on changes in parameters and grid configurations.

8. ACKNOWLEDGMENTS

This work is supported by NordForsk's Nordic University Hub Nordic Sound and Music Computing Network NordicSMC, project number 86892.

9. REFERENCES

[1] G. Borin, G. De Poli, and A. Sarti, "A modular approach to excitator-resonator interaction in physical models syntheses," in *Proceedings of the International Computer Music Conference*, 1989.

[2] J. Gomm, "Passionflower," 2011, [Online]. Available: https://www.youtube.com/watch?v=nY7GnAq6Znw.

[3] S. Bilbao, *Numerical Sound Synthesis*, John Wiley & Sons, United Kingdom, 2009.

[4] S. Willemsen, N. Andersson, S. Serafin, and S. Bilbao, "Real-time control of large-scale modular physical models using the sensel morph," in *Proc. of the 16th Sound and Music Computing Conference*, 2019, pp. 275–280.

[5] S. Willemsen, S. Bilbao, M. Ducceschi, and S. Serafin, "A physical model of the trombone using dynamic grids for finite difference schemes," submitted to *Proc. of the 23rd Int. Conf. on Digital Audio Effects (DAFx)*, 2021.

[6] J. D. Morrison and J.-M. Adrien, "Mosaic: A framework for modal synthesis," *Computer Music Journal*, vol. 17, no. 1, pp. 45–56, 1993.

[7] S. Mehes, M. van Walstijn, and P. Stapleton, "Towards a virtual-acoustic string instrument," in *Proceedings of the 13th Sound and Music Computing Conference (SMC)*, 2016.

[8] S. Willemsen, S. Serafin, and J. R. Jensen, "Virtual analog simulation and extensions of plate reverberation," in *Proc. of the 14th Sound and Music Computing Conference*, 2017, pp. 314–319.

[9] J.O. Smith, "Physical modeling using digital waveguides," *Computer Music Journal*, vol. 16, no. 4, pp. 74–91, 1992.

[10] R. Michon and J.O. Smith, "A hybrid guitar physical model controller: The BladeAxe," in *Proceedings ICMC\SMC\2014*, 2014.

[11] J. Strikwerda, *Finite Difference Schemes and Partial Differential Equations*, Wadsworth & Brooks/Cole Advanced Books & Software, Pacific Grove, California, 1989.

[12] S. Bilbao, "A modular percussion synthesis environment," in *Proc. of the 12th Int. Conference on Digital Audio Effects (DAFx)*, 2009.

[13] E. Zwicker and H. Fastl, *Psychoacoustics: Facts and Models*, Springer-Verlag, Berlin-Heidelberg, Germany, 1990.

[14] G. F. Carrier, "On the non-linear vibration problem of the elastic string," *Quarterly of Applied Mathematics*, vol. 3, pp. 157–165, 1945.